

Optimizing the acoustic properties of a meta-material using machine learning techniques

*Original*

Optimizing the acoustic properties of a meta-material using machine learning techniques / Casaburo, A., Magliacano, D., Petrone, G., Franco, F., DE ROSA, S.. - (2021). (Internoise 2021 Washington, USA 1 - 5 August 2021).

*Availability:*

This version is available at: 11583/2989032 since: 2024-05-27T16:44:10Z

*Publisher:*

The Institute of Noise Control Engineering of the USA, Inc.

*Published*

DOI:

*Terms of use:*

This article is made available under terms and conditions as specified in the corresponding bibliographic description in the repository

*Publisher copyright*

(Article begins on next page)



# Optimizing the acoustic properties of a meta-material using machine learning techniques

Alessandro Casaburo<sup>1</sup>  
Dario Magliacano<sup>2</sup>  
Giuseppe Petrone<sup>3</sup>  
Francesco Franco<sup>4</sup>  
Sergio De Rosa<sup>5</sup>

PASTA-Lab (Laboratory for Promoting experiences in Aeronautical Structures and Acoustics)  
Department of Industrial Engineering - Aerospace Section, Università degli Studi di Napoli  
"Federico II", Via Claudio 21, 80125 Naples, Italy

## ABSTRACT

*The scope of this work is to consolidate research dealing with vibroacoustics of periodic media. This investigation aims at developing and validating tools for the design of global vibroacoustic treatments based on foam cores with embedded periodic patterns, which allow passive control of acoustic paths in layered concepts. Firstly, a numerical test campaign is carried out by considering some solid (but still non-perfectly rigid) inclusions in a 3D-modeled porous structure; this causes the excitation of additional acoustic modes due to the periodic nature of the meta-core itself. Then, some design guidelines are provided in order to predict several possible sets of characteristic parameters (i.e. unit cell dimension and foam airflow resistivity) that, constrained by the imposition of the total thickness of the acoustic package, may satisfy the target functions (i.e. the frequency at which the first Transmission Loss peak appears, together with its amplitude). Results are obtained through the implementation of machine learning algorithms, which may constitute a good basis in order to perform preliminary design considerations that could be interesting for further generalizations.*

## 1. INTRODUCTION

Nowadays, present-day urbanization and traffic growth could seriously threaten human health, inducing annoyance, sleep disturbance, or even ischemic heart diseases [1], therefore the interest on environment noise reduction is quickly growing. In this context, porous media for acoustic purposes are materials made of channels, cracks or cavities, in which sound waves pass through the foam and lose energy due to viscous and thermal effects [2, 3]. However, porous media are not so efficient at low frequencies as they are at the high ones [4]. Such limitation is generally bypassed through the use of multi-layer arrangements [5]; in any case, the effects of these solutions always rely on the

---

<sup>1</sup>alessandro.casaburo@unina.it

<sup>2</sup>dario.magliacano@unina.it

<sup>3</sup>giuseppe.petrone@unina.it

<sup>4</sup>francesco.franco@unina.it

<sup>5</sup>sergio.derosa@unina.it

allowable thickness or on the total mass of the soundproofing configuration [6, 7].

In order to overcome such a constraint, low frequency performance of acoustic packages can be significantly enhanced by resorting to the use of porous media with embedded periodic inclusions [8,9]. Such a configuration provides proper dynamic filtering effects to the material, which could be beneficial for both the system dynamics and manufacturing. This approach may be suitable for different applications, such as energy, civil and transportation (aerospace, automotive, railway) engineering fields, where space, weight and acoustic comfort still represent key aspects.

Recently, an increasing research effort has been dedicated to analyze the transmission and dispersion properties of periodic acoustic meta-materials, characterized by the presence of local resonators. Novel functional applications of such research are expected in the optimal parametric design of smart tunable mechanical filters and directional waveguides, involving the use of machine learning techniques [10]. To this aim, both genetic algorithm and neural networks models are adopted in literature [11], representing an effective approach in order to design meta-materials. In particular, as an efficient machine learning method, deep learning has been widely used for data classification and regression in recent years, showing good generalization performance [12]. In general, compared with the traditional design process, using machine learning to guide the design of meta-materials can achieve faster, more accurate, and more convenient purposes.

Gaussian processes are chosen as machine learning method for this work, mainly due to their suitability to regression problems. In the second place, but not less importantly, Gaussian processes are mathematically equivalent to many well known models (like Bayesian linear models) and closely related to others, such as support vector machines. Moreover, the model provided is easier to handle and interpret than other counterparts and, at the same time, the method itself is easier to apply practically (it is not required to take plenty of decisions like architecture, activation functions, learning rate, etc.).

This work is structured as follows. First of all, the theoretical frameworks related to the characterization of the meta-material (Section 2.1) and to the chosen machine learning method (Section 2.2) are provided. In Section 3.1, it is illustrated a procedure, in the form of a MATLAB script, that allows to analytically calculate the required values of foam airflow resistivity and unit cell dimension in order to reach a desired target in terms of periodic resonance frequency, under specified constraints. Successively, in Section 3.2, the properties of the studied acoustic package, represented by an arrangement of periodic porous unit cells with perfectly rigid inclusions, are introduced, together with the 3-dimensional finite element (FE) geometries, and a parametric test campaign is performed for several setups, each with different values of foam airflow resistivity and unit cell dimension; for each of these cases, the sound transmission loss (TL) is estimated through different approaches, such as the Transfer Matrix Method (TMM) [13], in the case of homogeneous configurations, and the Finite Element Method (FEM) [14], in the case of meta-configurations. Then, in Section 3.3, a Gaussian-based machine learning algorithm is developed and applied in order to predict, with an error smaller than 5%, the TL increases at the resonance frequencies. In conclusions, in Section 4, the results of this investigation are commented, and some possible future expansions of the present research are evaluated.

## **2. THEORETICAL FRAMEWORK**

### **2.1. Characterization of the foam**

The phase decoupling frequency is defined as the frequency for which the inertial effects of the solid phase are equal, in magnitude, to the viscous effects of the fluid part. If one considers a foam, excited by an acoustic load at a frequency much higher than the phase decoupling one, with a stiffness (or a weight) much greater than the one of the air, the material frame can be considered as rigid and motionless [15]. Therefore, the porous medium with motionless skeleton can be replaced by the homogeneous fluid layer without modifying the reflected field in the external medium [13]. Two

classes of equivalent fluid models (i.e. expressions of complex density  $\rho$  and bulk modulus  $K$  as functions of the frequency and of the pore shape) can be listed [15]:

- Empirical models, which generally require the knowledge of a small number of parameters (or information); even if they are based on approximating assumptions, they are still very popular and very used.
- Semi-phenomenological models, which have been formulated for more complex pore morphologies; for this class of models, only the asymptotic behaviors are known, while a behavior between these asymptotes is assumed without being mathematically proven.

Among the first of the aforementioned models, from a large number of measurements on porous materials with porosities close to 1, Delany and Bazley [16] have proposed empirical expressions for the values of the complex wave number  $k$  and characteristic impedance  $Z_c$  for such materials:

$$Z_c = \rho_0 c_0 \left[ 1 + 9.08 \left( 10^3 \frac{f}{\sigma} \right)^{-0.75} - j 11.9 \left( 10^3 \frac{f}{\sigma} \right)^{-0.73} \right], \quad (1)$$

$$k = \frac{\omega}{c_0} \left[ 1 + 10.8 \left( 10^3 \frac{f}{\sigma} \right)^{-0.7} - j 10.3 \left( 10^3 \frac{f}{\sigma} \right)^{-0.59} \right], \quad (2)$$

where  $\rho_0$  is the density of air,  $c_0$  is the speed of sound in air,  $f$  is the frequency and  $\omega$  is the angular frequency. Boundaries, proposed by the authors, for the validity of these power law expressions are  $0.01 < \frac{f}{\sigma} < 1.00$ . This empirical model, which can provide reasonable estimations of  $k$  and  $Z_c$  in the approximate frequency range defined above, is still widely used for its simplicity: only one parameter, the airflow resistivity  $\sigma$ , is needed to describe the acoustic behavior of a material.

The model by Delany-Bazley-Miki [17] presents revised expressions for the complex wave number  $k$  and characteristic impedance  $Z_c$  of Delany-Bazley model [16]. In the case of multi-layers, Miki noticed that the real part of the surface impedance, when estimated with the classical Delany-Bazley model, may turn negative at low frequencies, thus leading to a non-physical result. In this context, Miki suggests the usage of the following expressions:

$$Z_c = \rho_0 c_0 \left[ 1 + 5.5 \left( 10^3 \frac{f}{\sigma} \right)^{-0.632} - j 8.43 \left( 10^3 \frac{f}{\sigma} \right)^{-0.632} \right], \quad (3)$$

$$k = \frac{\omega}{c_0} \left[ 1 + 7.81 \left( 10^3 \frac{f}{\sigma} \right)^{-0.618} - j 11.41 \left( 10^3 \frac{f}{\sigma} \right)^{-0.618} \right]. \quad (4)$$

The validity of Miki model is the same of that related to the original formulation, even if his revised expressions behaves well in a larger frequency range, in particular for  $\frac{f}{\sigma} < 0.01$ .

## 2.2. Gaussian processes

Stochastic processes can be briefly defined as the generalization of random variables to functions. More precisely, they are collections of random variables indexed by the input vector  $\mathbf{x}$  [18]. Thus, if  $\mathbf{x}_1, \mathbf{x}_2, \dots, \mathbf{x}_N$  are the  $d$ -dimensional training data points, a process is defined by the joint probability density of any finite subset  $(Y(\mathbf{x}_1), \dots, Y(\mathbf{x}_k))$  (with  $k < N$ ). A Gaussian process is a stochastic process whose joint density function is Gaussian and, therefore, completely defined by its mean and co-variance.

If the training data set is made of  $n$  ordered pairs  $(\mathbf{x}_1, t_1), \dots, (\mathbf{x}_n, t_n)$ , where  $t_i$  is a sample from a random variable  $T(\mathbf{x}_i)$ , then a prediction  $T^*$  at a new input  $\mathbf{x}^*$  is given by the conditional distribution  $p(T^* | T_1, \dots, T_N)$ . It can be demonstrated that the predicted mean and co-variance at  $\mathbf{x}^*$  are given by:

$$E[T^*] = \mathbf{k}^* \mathbf{K}^{-1} \mathbf{t}, \quad (5)$$

$$\text{var}[T^*] = k^* - \mathbf{k}^T \mathbf{K}^{-1} \mathbf{k}, \quad (6)$$

where  $\mathbf{k}$  denotes the co-variance vector of the training set (TS),  $k^*$  the co-variance of the new input  $\mathbf{x}^*$ ,  $\mathbf{K}$  the co-variance matrix, and  $\mathbf{t}$  the vector of the samples from the random variable  $T\mathbf{x}_i$ .

For simplicity, it is assumed that the Gaussian process has zero mean, therefore it is necessary to define just the co-variance between two points  $\mathbf{x}$  and  $\mathbf{x}'$ ; this is done with the co-variance function  $C(\mathbf{x}, \mathbf{x}')$ . Such a function is a crucial element in a Gaussian process predictor, as it encodes the assumptions about the function to learn in terms of similarity between data points (close points are more likely to have similar target values, hence training points close to a test points should be informative about the prediction at that point).

The co-variance function chosen in this work is the squared exponential, one of the probably the most widely-used co-variance function. Basically, it represents the exponential of a weighted squared distance between points in  $\mathbb{R}^d$ , so that vectors close in the input space give rise to highly correlated outputs:

$$C(\mathbf{x}^{(i)}, \mathbf{x}^{(j)}) = v_0 e^{-\frac{1}{2} \sum_{l=1}^d a_l (x_l^{(i)} - x_l^{(j)})^2} + b. \quad (7)$$

The term  $v_0$  controls the amplitude of the process, and  $b$  is a bias term related to the vertical offset. The term  $a_l$  weights the importance of the dimension under consideration (for example, if it is small, then the  $l$ -th input is down-weighted). Obviously, it is unrealistic to assume the knowledge of all the co-variance parameters *a priori*. It is, therefore, useful to start with a guess and adapt the values of these parameters to the training data set. This operation is carried out by means of scaled conjugate gradient optimization unskip [18], which suitably modulates the co-variance parameters once a random, initial guess is provided.

### 3. ANALYSES AND RESULTS

#### 3.1. Analytic part: calculation of the periodic resonance frequency

In this section, it is illustrated how Eq. 4 is inverted in order to estimate the required foam airflow resistivity  $\sigma$  for a desired resonance frequency. First of all, it should be pointed out that the resonance physics that is exploited herein, is linked to the well-known phenomenon that occurs when half the wavelength is equal to the periodicity dimension (i.e. the unit cell dimension). So told, Eq. 4 essentially involves four quantities: the wavenumber  $k$ , the frequency  $f$  (and thus the angular frequency  $\omega = 2\pi f$ ), the speed of sound in air  $c_0$  (that, in this context, can be considered as a constant value), and the foam airflow resistivity  $\sigma$ . Normally, such quantities are linked to each other such that the first one is the output, while the others are treated as inputs. In order to explicit the wavelength  $\lambda$ , which is required for the aforementioned reason, the wavenumber  $k$  is expressed as  $k = \frac{2\pi}{\lambda}$ ; then, since in correspondence of a periodic resonance it is verified that  $\frac{\lambda}{2} = d$  (where  $d$  is the dimension of periodicity), in that case one may write that  $k = \frac{\pi}{d}$ . At this point, considering that the real part of a complex wavenumber is generally linked to the propagation of the wave, while the imaginary one is related to its dissipation, for the purpose of the present analysis only the real part may be taken into account. Therefore, by neglecting the imaginary part of Eq. 4 and applying the aforementioned substitutions, in correspondance of a periodic resonance one obtains:

$$\sigma = 36.1 f \left( \frac{c_0}{2df} - 1 \right)^{1.618}. \quad (8)$$

The MATLAB script, based on Eq. 8, initially shows a prompt that asks for two geometrical constraints: the total available thickness, and the minimum unit cell dimension (which could be restrained by manufacturing aspects, and thus is limited by both lower and upper boundaries as shown in Figure 1); furthermore, the prompt also requires the input of a target resonance frequency, which could fall in the whole audible range. Then, starting from the combination of the two geometrical

constraints, the script calculates the possible numbers (and thus dimensions) of unit cells along the thickness; for each of them, the required  $\sigma$  at the assigned resonance frequency is computed through Eq. 8. Also the quantity  $\sigma$  is restrained in an interval, which in this case is lead by the material properties of common industrial foams, falling in the range between 3000 and 30000 [kg/(s\*m<sup>3</sup>)]. In this configuration, the script may display one or more (or even none) possible combinations of unit cell dimensions and airflow resistivity that, from a practical point of view, may lead to the choice respectively of a specific periodic pattern and foam material, with the aim of obtaining an acoustic resonance at the desired frequency.

Figure 1: Input prompt of the MATLAB script that analytically estimates periodic resonance frequencies.

### 3.2. Finite Element part: parametric analysis about airflow resistivity and periodicity dimension

The FE model is constituted by a layer of foam, with embedded periodic inclusions with the shape of cylindrical holes with perfectly rigid walls (Figure 2); the choice of the inclusion geometry represent an example, and may eventually impact the amplitude and/or the shape of the TL resonance peak, but not its frequency (since this only depends on the foam properties and on the dimension of the periodicity). For what concerns the FE implementation, the module “Pressure Acoustics and Frequency Domain” of COMSOL MultiPhysics is used both as modeling environment and numerical solver. For all structures presented in this work, the mesh consists of tetrahedral elements, generated through physics-controlled algorithms that are pre-implemented in the software, whose average number through models with different sizes is around 14250. Since the analyses are carried out considering an excitation consisting of a normal incidence plane wave acting on a layer of air (whose properties are reported in Table 1) along  $z$ -axis, the only fundamental boundary condition to apply is the so-called Perfectly Matched Layer (PML) on the very bottom face of the models: indeed, this represents an artificial absorbing layer for wave equations, commonly used to truncate computational regions in numerical methods in order to simulate problems with open boundaries; this allows the PML to strongly absorb outgoing waves from the interior of a computational region, without reflecting them back into the interior. On the contrary, boundary conditions applied on faces normal to  $x$ - and  $y$ - axes are not relevant for analyses with the above-mentioned kind of excitation, since under this condition the waves do not have propagating components along those directions; thus, for the sake of computational simplicity, a Sound Hard Boundary Wall (SHBW) boundary condition is applied herein. Eventually, for different angles of excitation, proper periodic conditions should be used instead. For a plane wave configuration at normal incidence  $\theta = \phi = 0$ , and thus oriented towards the negative direction of  $z$ -axis, the TL is computed as reported in Eq. 9.

$$TL = 10 \log_{10} \frac{\Pi_{incident}}{\Pi_{transmitted}}. \quad (9)$$

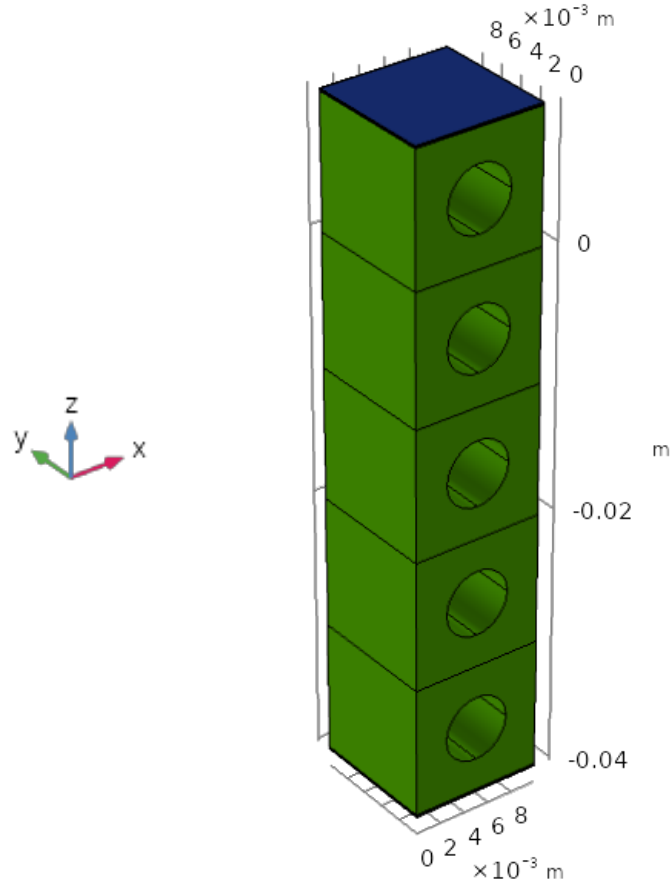


Figure 2: Example of FE geometry with five unit cells along the foam core thickness; the foam is green-colored, while the layers of air are blue-colored.

Table 1: Properties of air.

$\rho$ [kg/m <sup>3</sup> ]	1.213
Speed of sound [m/s]	3.42E+02

In the context of this work, the TLs related to the homogeneous (which, obviously, has no inclusions) and the meta-core models are respectively estimated through a TMM implementation of Eq. 10 and Eq. 11, and an FE solution of Eq. 9.

$$TL = 10\log_{10}\left(\frac{1}{4}|T_{11} + \frac{T_{12}}{\rho_0 c_0} + \rho_0 c_0 T_{21} + T_{22}|^2\right), \quad (10)$$

$$\text{with } \begin{bmatrix} T_{11} & T_{12} \\ T_{21} & T_{22} \end{bmatrix} = \begin{bmatrix} \cos(kd) & j \sin(kd)Z_c \\ \frac{j \sin(kd)}{Z_c} & \cos(kd) \end{bmatrix}. \quad (11)$$

A parametric analysis is performed for all possible combinations of two chosen sets of foam airflow resistivity and unit cell dimension values. In particular, 12 airflow resistivities (from 3000 to 30000 [kg/(s\*m<sup>3</sup>)]) and 10 unit cell dimensions (from 0.01 to 0.025 [m]) are selected, both on a logarithmic scale, for a total of 120 different test cases; for each of them, the periodic resonance frequency (Figure 3) is analytically calculated through the approach illustrated in Section 3, while the TL percentage increase (Figure 4) related the meta-core solution, compared to its homogeneous counterpart at fixed

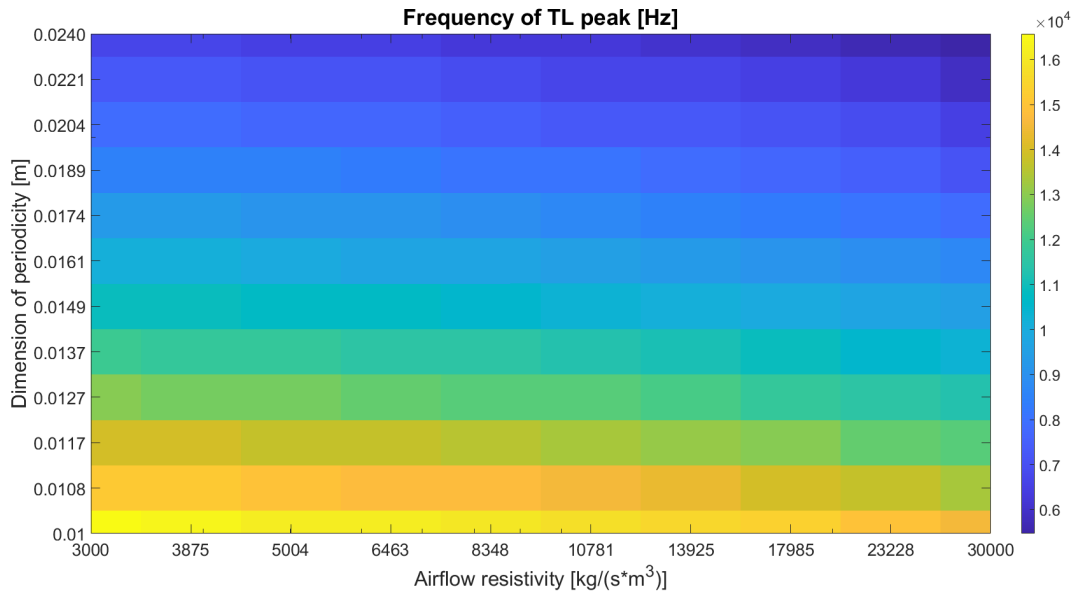


Figure 3: Transmission Loss frequency behavior as a function of unit cell dimension and foam airflow resistivity.

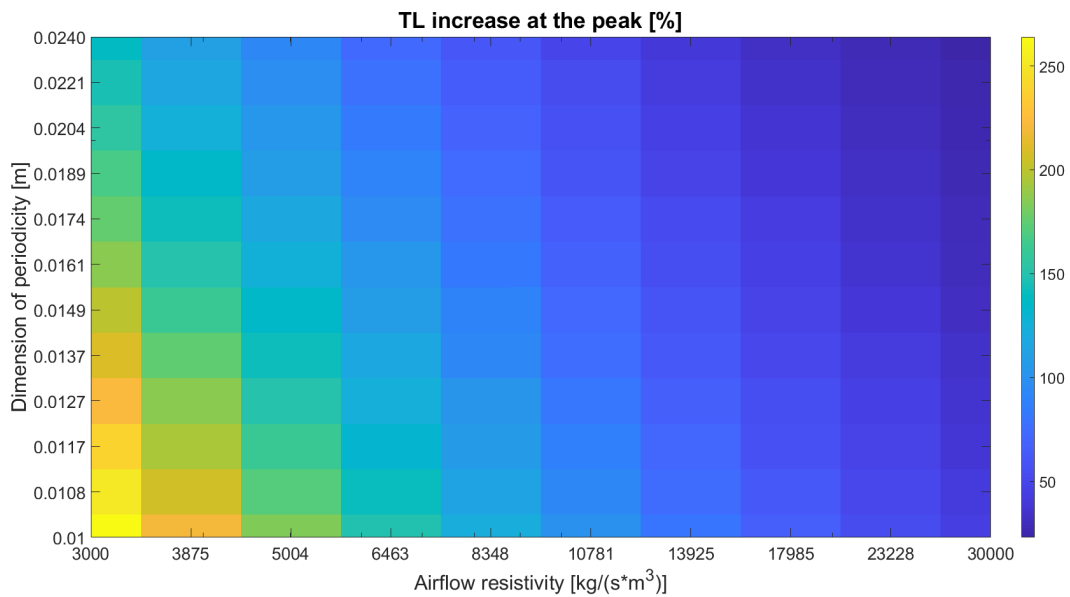


Figure 4: Transmission Loss increase behavior as a function of unit cell dimension and foam airflow resistivity.

total thickness, is numerically estimated in COMSOL environment using Eq. 9 and 10. For example, considering a couple of  $\sigma$  and  $d$  values respectively equal to 5004 [kg/(s\*m³)] and 0.0127 [m], from Figure 3 it may be found a resonance frequency around 13000 [Hz] (the analytical value is 12735 [Hz]), while from Figure 4 it may be estimated an increase in the TL amplitude peak of around 150% (the FE value is 151%); instead, considering a couple of  $\sigma$  and  $d$  values respectively equal to 17985 [kg/(s\*m³)] and 0.0189 [m], from Figure 3 it may be found a resonance frequency around 8000 [Hz] (the analytical value is 7689 [Hz]), while from Figure 4 it may be estimated an increase in the TL amplitude peak of around 50% (the FE value is 40%).

### 3.3. Machine Learning part: prediction of the Transmission Loss increase at the resonance frequency

As previously mentioned, the objective is to predict the TL increase peak in an automated way with a machine learning method, namely Gaussian processes. As mentioned in Section 2, the predictions on new instances are given by Eq. 5, and the estimation of the hyper-parameters is carried out with an optimization algorithm. Therefore, once the co-variance function is decided, Gaussian processes do not need any user-defined choice other than the number of training examples. Since the generation of both a numerical and/or experimental training set would be time consuming and financially expensive, it is tried to carry out the prediction of new instances by using the lowest number of training examples as possible; such a prediction would be considered satisfying if the percent error between the numerical and predicted peak reduction is below 5%. Moreover, in order to demonstrate the robustness of the method with the chosen number of examples, in the problem at hand, the predictions are made with three different training sets, called TS1, TS2, and TS3. To this aim, the 120 test cases numerically obtained are used as pool from which to extract training and test examples. In particular, the complete observation of each sample is made of four features: airflow resistivity, unit cell dimension, and resonance frequency as input, while the TL peak decrease is, obviously, the output. The three sets share 20 samples, which describe the boundaries of the input space (to avoid extrapolation), to which other examples are randomly added from the aforementioned pool. The remaining elements are used for testing the generalization capabilities of the method. Before proceeding with the learning, feature scaling is executed on all the training samples as:

$$x'_i = \frac{x_i - \mu}{\sigma_{std}}, \quad (12)$$

where  $x_i$  and  $x'_i$  are the original  $i$ -th feature and the scaled one, respectively,  $\mu$  is the mean value of the feature, and  $\sigma_{std}$  is the standard deviation of the feature, both evaluated on the whole training set. This operation is almost mandatory, since the different orders of magnitude of the parameters involved may generate numerical problems during learning. Feature scaling, instead, reduces all the features to the same order of magnitude. After learning, the features are then descaled, so that the results of the predictions are made understandable to the user.

The results provided by Gaussian processes are summarized in Figure 5. Each row displays, on the left, a 3D plot relating the three inputs (airflow resistivity, unit cell dimensions, and resonance frequency), on the cartesian axis, and the predicted peak decrease (color-coded) corresponding to each coordinate. On the right, 2D plots link the independent variables ( $\sigma$ ,  $d$ ) (which provide frequency according to Eq. 4) to the corresponding prediction error. In these figures, the black dots indicate the training examples, that must not be considered for the performance evaluation of the machine learning method.

Concerning these performances, the 2D plots show that, with a training set made of 45 samples, the prediction error remains inside the 5% boundary. The distribution of the higher errors does not follow a predictable pattern, since they not only appear in the central region of the map, but also close to the boundaries and, sometimes, training examples. However, the same considerations hold for the lower errors. In order to have a greater insight on the performances of Gaussian processes, three test cases are considered: the analytical and numerical TL curves are provided in Figure 6 (where the Frequency axis is cut at 14000 [Hz], in order to better visualize the curves and the related peaks), while Table 2 summarizes the results in terms of reference amplitude, predicted amplitude, and prediction error for all the three training sets. Table 2 highlights the excellent performances of Gaussian processes. More generally, TS1, TS2, and TS3 exhibit a mean percent error equal to 1.49, 1.42, and 1.66, respectively, which is much lower than the 5% boundary fixed.

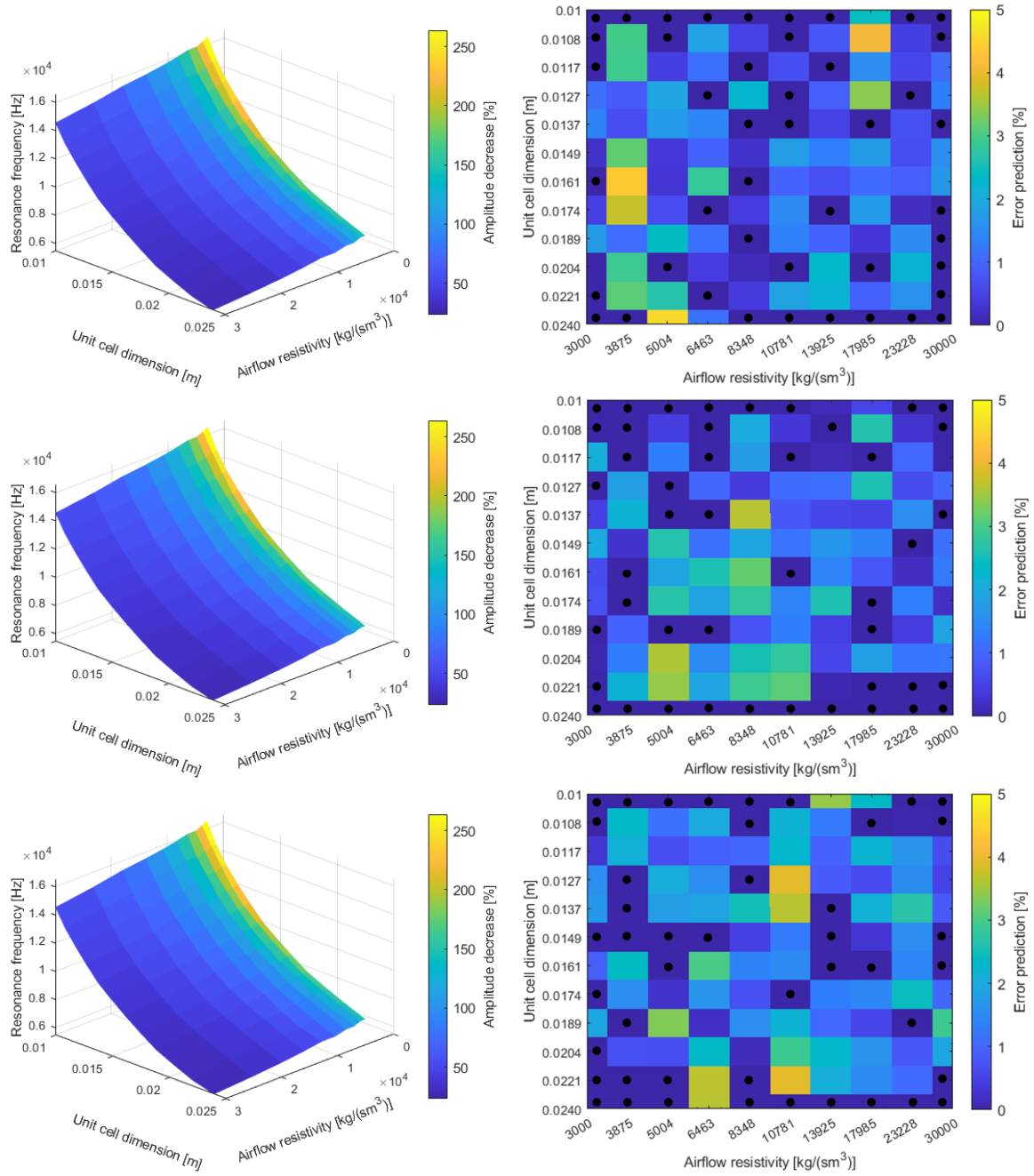


Figure 5: On the left, from top to bottom, 3D plots that relate the three inputs of the machine learning algorithm to the predicted TL amplitude percentage increase at the resonance peaks (coded in the colorbar), for each of the three tested TSs. On the right, from top to bottom, 2D plots that relate the two mutually independent inputs of the machine learning algorithm to the percentage error about the prediction of TL amplitude percentage increase at the resonance peaks (coded in the colorbar), for each of the three tested TSs; values marked with black points are those used as training set, while all the remaining ones constitute the actual test set.

#### 4. CONCLUSIONS

The scope of this work is to develop and validate tools for the design of global vibroacoustic treatments based on foam cores with embedded periodic patterns, through the implementation of machine learning algorithms, which may constitute a good basis in order to perform preliminary design considerations that could be interesting for further generalizations.

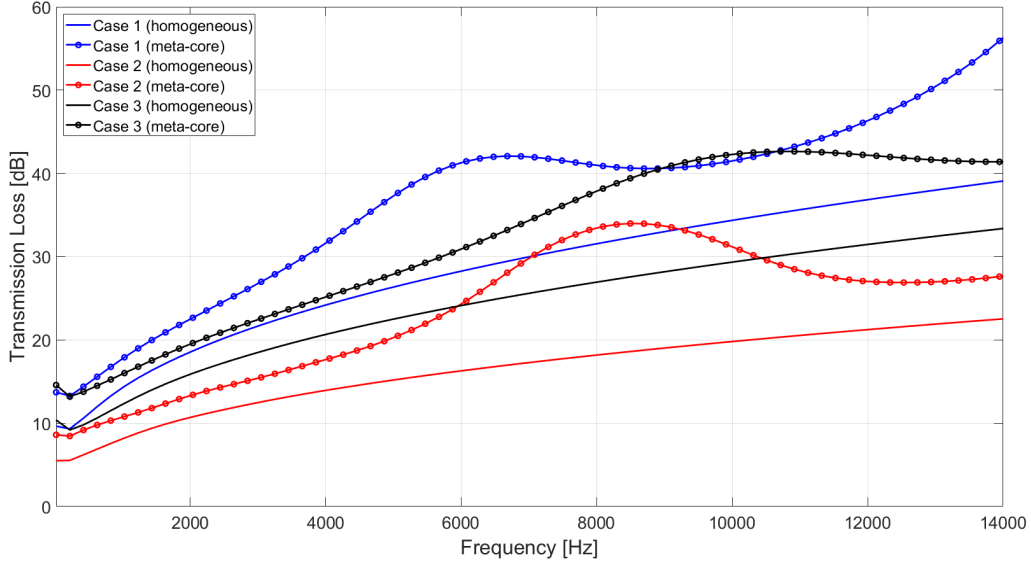


Figure 6: Transmission Loss analytically and numerically computed, respectively through TMM and FE approaches, for 3 test cases with different combinations of airflow resistivity and unit cell dimension; further details about Case 1, Case 2 and Case 3 are reported in Table 2.

Table 2: Amplitude increments at the resonance peaks and related errors for three tested  $(\sigma, d)$  couples, predicted through three different training sets.

	<b>Case 1</b>	<b>Case 2</b>	<b>Case 3</b>
$(\sigma, d)$	(13925, 0.022)	(8348, 0.0174)	(23228, 0.0137)
<b>Resonance frequency [Hz]</b>	6680	8900	10515
<b>Amplitude increment (FEM) [%]</b>	42.38	78.09	42.17
<b>Amplitude increment (TS1) [%]</b>	42.32	79.22	41.61
<b>Error on amplitude increment (TS1) [%]</b>	0.13	1.44	1.33
<b>Amplitude increment (TS2) [%]</b>	42.66	79.42	41.72
<b>Error on amplitude increment (TS2) [%]</b>	0.66	1.70	1.06
<b>Amplitude increment (TS3) [%]</b>	42.69	79.40	41.31
<b>Error on amplitude increment (TS3) [%]</b>	0.72	1.67	2.04

First of all, the theoretical frameworks related to the characterization of the meta-material and to the chosen machine learning method are provided. Then, it is illustrated a procedure that allows to analytically calculate the required values of foam airflow resistivity and unit cell dimension in order to reach a desired target in terms of periodic resonance frequency, under specified constraints. Successively, the properties of the studied acoustic package are introduced, together with the 3-dimensional finite element geometries, and a parametric test campaign is performed for several

setups, each with different values of foam airflow resistivity and unit cell dimension. In conclusion, a Gaussian-based machine learning algorithm is developed and applied in order to predict, with an error smaller than 5%, the Transmission Loss increases at the resonance frequencies.

Future expansions of the present work may involve the development and implementation of an advanced analytical formulation for the prediction of geometrical and material properties in order to reach a target resonance frequency, based on the modeling of the foam though more accurate and complex equivalent fluids. Moreover, it could be relevant to adopt more advanced machine learning techniques, not only for the estimation of the acoustic performance of meta-materials, but even for their choice and optimization, according to the applications of interest.

## ACKNOWLEDGMENTS

The authors acknowledge the support of the Italian Ministry of Education, University and Research (MIUR) through the project DEVISU, funded under the scheme PRIN-2107 – grant agreement No. 22017ZX9X4K006.

## REFERENCES

- [1] L. Cao, Q. Fu, Y. Si, B. Ding, and J. Yu. Porous materials for sound absorption. *Composite Communications*, 10:25–35, 2018.
- [2] U. Berardi and G. Iannace. Acoustic characterization of natural fibers for sound absorption applications. *Building Environments*, 94:840–852, 2015.
- [3] X. Xinzhao, L. Guoming, L. Dongyan, S. Guoxin, and Y. Rui. Electrically conductive graphene-coated polyurethane foam and its epoxy composites. *Composite Communications*, 7:1–6, 2018.
- [4] J.-P. Groby, B. Nennig, C. Lagarrigue, B. Brouard, O. Dazel, and et al. Using simple shape three-dimensional inclusions to enhance porous layer absorption. *Journal of Acoustical Society of America*, 136(3):1139–1148, 2014.
- [5] Y. Yang, B.R. Mace, and M.J. Kingan. Wave and finite element method for predicting sound transmission through finite multi-layered structures with fluid layers. *Computers and Structures*, 204:20–30, 2018.
- [6] T. Weisser. Acoustic behavior of a rigidly backed poroelastic layer with periodic resonant inclusions by a multiple scattering approach. *Journal of Acoustical Society of America*, 139(2):617–629, 2016.
- [7] M. Gaborit, O. Dazel, and P. Göransson. A simplified model for thin acoustic screens. *Journal of Acoustical Society of America*, 144(1):76–81, 2018.
- [8] J.-P. Groby, A. Wirgin, L. De Ryck, W. Lauriks, R.P. Gilbert, and Y.S. Xu. Acoustic response of a rigid-frame porous medium plate with a periodic set of inclusions. *Journal of Acoustical Society of America*, 126(2):685–693, 2009.
- [9] L. Xiong, B. Nennig, Y. Aurégan, and W. Bi. Sound attenuation optimization using metaporous materials tuned on exceptional points. *Journal of Acoustical Society of America*, 142(4):2288–2297, 2017.
- [10] A. Bacigalupo, G. Gnecco, M. Lepidi, and L. Gambarotta. Machine-learning techniques for the optimal design of acoustic metamaterials. *Journal of Optimization Theory and Applications*, 187(3):630–653, 2020.
- [11] L. Wu, L. Liu, Y. Wang, Z. Zhai, H. Zhuang, D. Krishnaraju, Q. Wang, and H. Jiang. A machine learning-based method to design modular metamaterials. *Extreme Mechanics Letters*, 36, 2020.
- [12] Z. Hou, T. Tang, J. Shen, C. Li, and F. Li. Prediction network of metamaterial with split ring resonator based on deep learning. *Nanoscale Research Letters*, 15(1), 2020.

- [13] J.F. Allard and N. Atalla. *Propagation of sound in porous media: Modelling sound absorbing materials*. Wiley, 2<sup>nd</sup> edition, 2009.
- [14] D. Magliacano, M. Ouisse, S. De Rosa, F. Franco, and A. Khelif. Computation of acoustic properties and design guidelines of periodic biot-modeled foams. *Applied Acoustics*, 168, 2020.
- [15] M.R. Stinson. The propagation of plane sound waves in narrow and wide circular tubes, and generalization to uniform tubes of arbitrary cross-sectional shape. *Journal of the Acoustical Society of America*, 89(2):550–558, 1991.
- [16] M.E. Delany and E.N. Bazley. Acoustical properties of fibrous absorbent materials. *Applied Acoustics*, 3(2):105–116, 1970.
- [17] Y. Miki. Acoustical properties of porous materials: Modifications of delany-bazley models. *Journal of the Acoustical Society of Japan (E)*, 11(1):19–24, 1990.
- [18] I.T. Nabney. *Netlab: Algorithms for Pattern Recognition*. Springer, 1<sup>st</sup> edition, 2002.